Gamma Ray Detector with Neutron Detection Capabilities for Shielded Fission Sources

Ashton C. Brown

A senior thesis submitted to the faculty of
Brigham Young University
in partial fulfillment of the requirements for the degree of

Bachelor of Science

Dr. Lawrence Rees, Advisor

Department of Physics and Astronomy

Brigham Young University

April 2017

ABSTRACT

Gamma Ray Detector with Neutron Detection Capabilities
for Shielded Fission Sources

Ashton C. Brown
Department of Physics and Astronomy, BYU
Bachelor of Science

With homeland security applications in mind, I constructed and tested a gamma ray and neutron detector designed to detect spontaneous fission events from highly shielded sources. The detector consisted primarily of a 25.4 cm $\times$ 25.4 cm $\times$ 15.2 cm block of Eljen EJ-200 plastic scintillator coupled to four Adit 5-inch photomultiplier tubes. The signals from all the tubes were added following gain matching with a ^{60}Co gamma source. Using a ^{252}Cf source, I measured the efficiency of the detector for various shielding types and thicknesses. Data were acquired both with a Cd foil placed on the front of the detector and with the Cd foil removed. The difference of the pulse-height histograms for these two configurations was shown to be a good measure of the neutron source strength. Neutron detection efficiency per fission neutron in a 4π detector peaked at 13.5%, corresponding to a shielding diameter of 20.4 cm. Through single and double pulse analysis, we were able to confidently determine if a fission source was present and also if boron was being used in the shielding.

Keywords: Fission, Gamma Ray Detector, Homeland Security, Neutron Detector, Radiation Portal Monitoring

ACKNOWLEDGMENTS

My deep thanks go to Bart Czirr, a mentor and friend. The privilege to work with him on this idea of his seemingly happened upon me. How grateful I am that it did! It has been a pleasure to learn from him, as he is a great teacher. It wasn't just physics that I learned either.

I would like to thank Dr. Larry Rees as well. He has taught me a great deal, and kept me on course in this project. I have especially enjoyed the laughs we have shared during our weekly research meetings.

My wife Courtney deserves my deepest appreciation. I have enjoyed running all the intricate details by her throughout the project's lifetime, though I am sure it was not as fun for her as it was for me. Thank you for supporting me in my studies.

Contents

List of Figures

List of Tables

Chapter 1

Introduction

1.1 Fission Detectors Along our Borders

The unfortunate but necessary game of protection we have had to play with terrorists has led to extensive radiation portal monitoring (RPM), a system designed to keep fissile materials from getting into the country through our ports. Elements that spontaneously fission, like specific isotopes of plutonium and uranium, are the explosive ingredient in atomic bombs. Fission sources emit gamma rays and neutrons, among other particles; so, neutron and gamma detectors are key in passively identifying and interdicting such bombs. Of these two particles, neutrons have become the focus. Thus, neutron detectors now span the country, enabling interdiction of fissile materials. The Department of Homeland Security (DHS) currently utilizes the ^{3}He detector. While it is a very reliable neutron detector, a replacement needs to be found, for this isotope of helium is in short supply.

As terrorists attempt to import fissile materials, the fission source will be shielded. Kouzes *et al*. [1] discuss the types of shielding that could be present whether by shipping default or by the design of the terrorist. Either way, their conclusions delineate the need for the RPM detectors

to be sensitive to not only bare sources, but also well-shielded sources. This paper presents the construction, testing, and results of a passive, polyvinyl-toluene-based gamma detector that has neutron detection capabilities for a wide range of source shielding.

1.2 Established Neutron-Detection Methods

Detecting neutrons proves difficult given their neutral nature. Knoll [2] gives great detail on methods and materials for neutron detection. Generally, there are two methods for neutron detection: energy transfer to charged particles and neutron capture in isotopes with high neutron-capture cross sections. For the first, the neutron transfers kinetic energy through collision to a charged particle, a proton (proton recoil) for example. The charged particle then excites the scintillator (part of the detector design), and the photons emitted by the scintillator can be detected by a photomultiplier tube (PMT). For the second, isotopes like ^{10}B or ^{6}Li, capture low energy neutrons and emit a gamma ray. This gamma ray then Compton scatters, and like the first method, the now-moving charged particle excites the scintillator and the PMT picks up the signal. For the case of ^{3}He, neutron capture occurs, the gas is ionized by the proton and triton created, and a pulse is picked up by a biased wire stretching the length of the gas tube.

For each method, the goal is to avoid false positives caused by gamma rays. Discriminating between neutrons and gammas has been key in detecting spontaneous fission, since gamma rays alone do not suffice. Therefore, these types of neutron detectors are designed to avoid unwanted sensitivity to ambient gamma rays. For the energy transfer method, materials are selected so that gamma rays (through Compton scattering) and neutrons (through proton recoil) each produce unique pulses. Pulse shape discrimination can then be used to identify the particle. For the capture method, the materials are selected so that the pulse height of a neutron capture event is much higher than gamma-induced pulses. Therefore they are in this case discriminated by pulse height.

Many other detectors utilize both interactions to discriminate and detect neutrons. Many of these detectors have therefore become quite sophisticated.

1.2.1 Methods Explored at Brigham Young University

At Brigham Young University (BYU), methods have been tested that have led to the current design. A common method among the Nuclear Research Group at BYU is identifying neutrons by looking for both proton recoil and neutron capture. This method (called capture gated detection) has been tested with a fourfold-PMT detector of polyvinyl toluene (PVT) and Cd foil. Projects have included calibration through time of flight measurements [3] and analysis of the ^{258}U fission spectrum [3]. A prototype with Adit PMT's has also been analyzed for efficiency versus neutron energy [4].

1.3 Gamma Ray Count: Our Approach

As mentioned, gamma sensitivity is traditionally avoided in RPM. In spite of this, our PVT-based detector is essentially a gamma detector, with intentional gamma sensitivity. This sensitivity, when used properly, provides unique capabilities in RPM. Let us consider the advantages of shifting the focus from the neutrons to the gamma rays. Firstly, the fission gamma is detectable. The fission gamma spectrum for any given source is partially above the DHS threshold standard, ^{60}Co gammas. Therefore, even for high thresholds like that of DHS, fission gammas are a good source for identifying fission. This cobalt requirement, set by DHS, is that no more than one in a million cobalt gamma rays can be misidentified as a neutron.

The second advantage is that signal is not lost, but enhanced when shielding is used. Typical neutron shielding consists of a lot of hydrogen. The hydrogen atom, of a mass nearly equal to that of the neutron, absorbs a lot of energy in a collision interaction. So with a very hydrogenous material, neutrons are moderated relatively quickly. Once they are thermalized, they can then be

completely eliminated from ever being detected by being captured. Hydrogen captures neutrons according to the following reaction:

$$n + p \rightarrow d + \gamma \ (2.2\,\text{MeV}). \tag{1.1}$$

Shielding can be enhanced when it is infused with elements with even higher neutron-absorption cross sections, like ^{10}B. This isotope of boron has a higher cross section than hydrogen by a factor of 10^4. Therefore, shielding is effective when boron is incorporated. Boron captures neutrons according to the following reaction:

$$n + {}^{10}B \rightarrow {}^{11}B + \gamma \ (0.477\,\text{MeV}). \tag{1.2}$$

Since we have a gamma detector, the loss of neutrons due to capture increases our gamma count. Both reactions (Equations (1.1) & (1.2)) create gamma rays that would otherwise never be detected because of gamma insensitivity. Though the boron capture gamma is of quite low energy, it still contributes to increasing gamma counts for thresholds below the DHS standard. More importantly, because of its large cross section for neutron capture, gamma rays can be used to find neutrons' time-to-capture, which would identify boron in the shielding. Accurately identifying boron in shielding would be a huge advantage in RPM.

The final advantage is found in the design of the detector. Neutrons that make it out of the shielding and to our detector have the chance to capture in a thin sheet of cadmium placed on the face of the detector. Cadmium captures neutrons according to the following reaction:

$$n + {}^{113}Cd \rightarrow {}^{114}Cd^* \rightarrow {}^{114}Cd + \gamma. \tag{1.3}$$

From this reaction, it is evident that even more gammas are created for our detector to pick up. Thus, the idea is to convert as much of the fission products as you can to gamma rays. During de-excitation, ^{114}Cd gives off about 9 MeV of energy in the form of gamma rays. Though the number of gammas emitted varies from capture to capture, the average energy of a single gamma

ray per capture is 1 MeV. Because the Cd sheet is on the face of the detector, half of the 9 MeV will be directed at the detector on average. So, not only are the fission and shielding capture gammas above energies of common gamma sources, but also the sum of these cadmium capture gammas heading at our detector.

A neutron signal can be found from removing the cadmium sheet from the detector face. Any difference in count rate between the 'on' configuration (Cd_{IN}) and the 'off' configuration (Cd_{OUT}) should be due to neutron capture gammas in the cadmium sheet. Therefore, the neutron signal is separated from the gamma signal by subtracting the Cd_{IN} counts from the Cd_{OUT} counts.

The sophistication of recent neutron detectors is contrasted by our detector. A large block of plastic scintillator and a sheet of cadmium is all it takes. No need to discriminate...no need for involved designs. Our detector adequately resolves the gamma spectrum and at the same time obtains a neutron count. This combination of abilities makes for a reliable *fission* detector.

Chapter 2

Methods

In order to obtain valid data, several aspects of preparation needed special attention. The detector needed to be properly assembled and secured in a light-tight box. To ensure constant parameters, the experiment was designed carefully; only the shielding size was to vary from run to run. Other preparations included gain matching the four PMT's and obtaining proper amplifier settings. These two preparations were accomplished with a cobalt-60 source. We chose the settings for the digitizer, and kept them constant as well. We obtained data meant for single-pulse analysis, which was used for calculating our detector's intrinsic efficiency. To explore detection capabilities, we also took data designated for double-pulse analysis.

2.1 Detector Design

The detector is of a simple and inexpensive design. The core of the detector is Eljen EJ-200 plastic scintillator. It is 25.4 cm $\times$ 25.4 cm $\times$ 15.2 cm in dimension, with the larger cross-sectional area as the face of the detector. Four Adit PMT's (model B133D01S) were coupled to the scintillator. Since PMT's are sensitive to light in the visible range, these five pieces were all secured in a light-tight aluminum box.

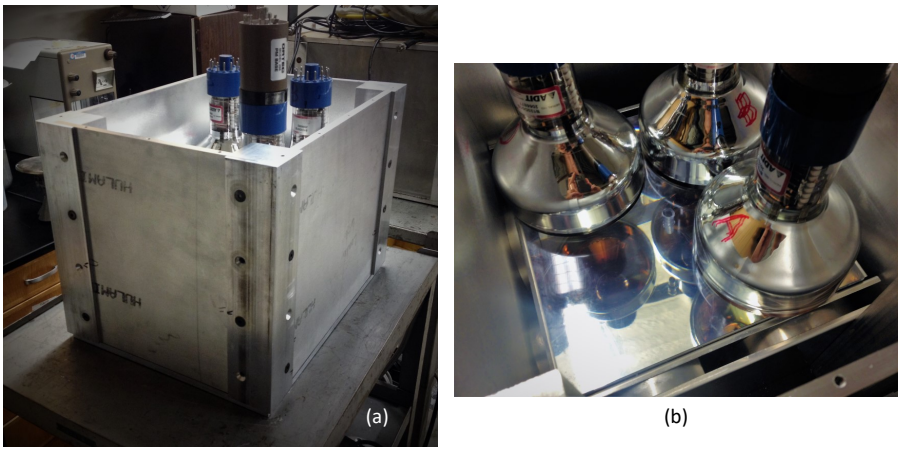

Figure 2.1 The detector in assembly. In (a), the detector is face down without the back lid on. The use of both the aluminum spacers and the aluminized mylar is demonstrated in (b). Three of the four PMT's are present in both pictures.

Assembly of the detector was also quite simple. To capture as much of the light from scintillation as possible, the plastic block was covered with aluminized mylar (reflective side inward) on all sides except the face designated for the PMT's. The plastic scintillator and mylar were secured in the light-tight box by aluminum spacers, which pinch the core in place. To improve transmission of light, the PMT faces and the plastic were joined with optical grease. Thin layers of black rubber optically sealed the joints of the aluminum box and O-rings the PMT holes. Figure 2.1 contains pictures of the detector during assembly.

2.2 Experimental Setup

Five basic parts constitute the experimental setup. These parts, found in Fig. 2.2, are: the source, the detector, the conversion of the detector response (light pulse) to an electrical pulse, amplification and attenuation of pulse, and conversion of the electrical pulse to digital data. The source was primarily ^{252}Cf, though ^{60}Co was used for gain-matching and amplification purposes. The californium source was consistently 20 inches from the center of the detector face. The gamma rays,

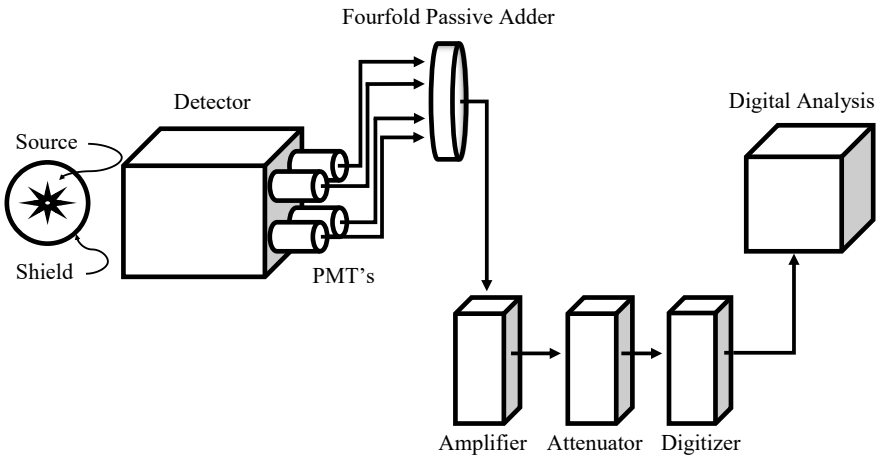

Figure 2.2 A schematic of the experimental setup. The detector picks up signals from the source. The four PMT signals are combined and sent through an amplifier. The amplifier and attenuator ensure that no signal will exceed a specified ceiling voltage, which protects the digitizer. Then the digitizer converts the signal into binary and the computer saves the data. The data are then ready for analysis.

whether directly from fission or from neutron capture in cadmium, Compton scatter in the plastic scintillator, causing scintillation. The light pulse from the scintillation then makes it to the PMT's, where the light is converted into an electrical pulse. The PMT's were powered by Ortec 556 High Voltage power supplies. The pulse then goes through the amplifier (Ortec 474 Timing Filter Amp) and attenuator. These two components work together to ensure the range of energy of particles we desire to detect (0 - 10 MeV) stretch across the range of voltage with which the digitizer can work (0 - 1 V). The digitizer (CAEN DT5720) converts the analog data to digital data (binary), and the computer stores the data. The data are then ready for pulse height analysis.

To determine our detector's intrinsic efficiency against source-shielding thickness, we made a set of our own shielding. The shielding we chose to use were spheres of varying diameters of paraffin wax. We took bars of wax, melted them down two or three at a time, and poured them into spherical shells (mostly basketball skins). Once the wax cooled and hardened, we melted and poured another two or three bars. We did this until the shells were full. We then drilled a

Figure 2.3 Pictures of making the source shielding, and the final product. We filled these balls with paraffin wax by melting several bars at a time over a hot plate and pouring the wax in the shell, shown in (a). We drilled a hole to the center in each, evident in (b). The source would be dropped in the sphere and data would be taken with the hole open at the top.

hole just wide and deep enough for the source to fall into the center of the wax sphere. Since the shell was plastic (and therefore hydrogenous like the wax), we left it on and counted it as part of the shielding thickness. We produced and used paraffin wax shields with diameters of 6.48, 12.41, 22.4, and 23.5 cm (see Fig. 2.3). Table 2.1 presents the shielding sizes with their respective masses, which quantities affect the expected neutron capture rate in the shielding.

Table 2.1 Paraffin wax shielding diameters and masses.

Shielding Diameter (cm)	Shielding Mass (kg)
6.48	0.121
12.61	0.973
20.4	4.00
23.5	7.44

2.3 Gain Matching the Photomultiplier Tubes

With four photomultiplier tubes coupled to the scintillator, energy resolution is lost when the PMT's do not respond uniformly to a given event. It is mandatory to balance, or gain match, the four PMT's so that their response to the same event is similar. Cobalt emits gamma rays of two distinct energies: 1.173 MeV and 1.332 MeV. Because of these distinct gamma energies, ^{60}Co served well in providing consistent events, leaving any discrepancy between the PMT's a matter of gain. Therefore, to gain match the four Adit PMT's, I exposed the detector to ^{60}Co for a minute with 1200 V of gain on one PMT while the others were off. I did this for each PMT, and then produced their respective pulse height histograms. With the pulse height spectra of these data all together, it is clear which PMT's need more gain and which need less, because the cobalt peak in the spectra *should* fall at the same pulse height. So, you adjust the gain accordingly, and repeat the process until the cobalt peaks all have the same pulse height. For our PMT's, the cobalt peaks best aligned with 1200 V to one PMT, 1240 V to another, and 1290 V to the last two. Because the detector has relatively low resolution, energies this close cause a single peak on a pulse-height histogram. This peak, indicating relatively low yet adequate resolution, is found in Fig. 2.4.

2.4 Amplifier Settings

The amplifier settings were determined in a way similar to the PMT's gain. To be able to compare sets of data, I had to ensure that a gamma ray of a given energy produced the same pulse amplitude from day to day. Therefore, the settings for the amplifier each day were determined using, again, ^{60}Co. I exposed the detector to cobalt for a minute and then looked at the pulse height histogram. If the cobalt peak was not in the proper pulse height bin, then I adjusted the gain on the amplifier, and took another minute of cobalt data. I repeated this process until the cobalt peak was in the designated bin. The bin was chosen so that the peak was of low pulse height (90 ± 5 mV), leaving

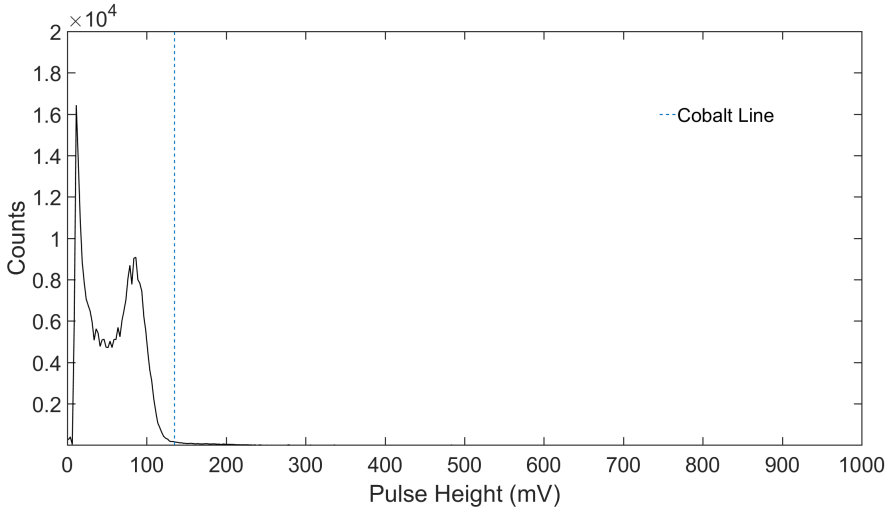

Figure 2.4 Pulse-height histogram of a one-minute run for the detector exposed to ^{60}Co. With the resolution of the detector, the two gamma rays from cobalt are close enough in energy that they produce one peak. Gain was always adjusted so that the center of the peak fell on 90 $\pm$ 5 mV. The cobalt line defines the DHS threshold for our settings.

room for the cobalt-free region (the white space to the right of the cobalt line in Fig. 2.4). The cobalt line in the figure is at 135 mV and represents the threshold used to satisfy the DHS cobalt-standard described in Section 1.3.

2.5 Data Acquisition

For runs designated for single-pulse analysis, I acquired data in 5 minute intervals. Every run is 5 $\pm$ 0.003 minutes. Despite the time variation being small, every pulse height histogram is normalized by its own run time, and then scaled to 5 minutes exactly. For every shielding size, a run was performed with the cadmium sheet taped on the face of the detector, and another without it. The digitizer settings (made in the configuration file) were all default except for the following specifications: The time limit was 300 s, the event limit was set to zero, the samples acquired per event was 512, the percent post trigger was 50, the event threshold was 15 half millivolts, and the dc offset was always adjusted so that background was 0.0 $\pm$ 0.75 mV.

For runs designated for double-pulse analysis, all aspects of the setup were the same except for a few settings in the digitizer configuration file: The samples acquired per event was 5000 and the percent post trigger was 98. For all of the specifications in the configuration files for the two types of runs, see Appendix A.

Room return is an effect that smothers data. Room return occurs when neutrons scatter off objects not intended to be part of the system and return to the detector to become part of your data. This is unwanted data, and can be avoided. Since neutrons and protons are of nearly equal mass, neutron clouds form readily in hydrogenous materials. This means that the more you can isolate your system from hydrogenous materials, like cement, the less an effect room return will have on your data.

Figure 2.5 (a): A picture of the stand for the source and shielding with the face of the detector visible. (b): A picture of the scissor lift partially extended (fully extended is about 20 feet from the ground). Data were acquired with the system on the scissor lift, fully extended, with the source 20 inches from the detector face.

For these reasons, we performed our runs outside, on a scissor lift (see Fig. 2.5). This put our system (the source, shield, and detector) 20 feet in the air, away from cement and other hydrogenous materials. The closest objects causing some room return were nearby trees. More details on avoiding room return can be found in Brian Ostler's thesis [5].

2.5.1 Background

Background runs were taken to check if background corrections were needed. If the backgrounds were to be the same for Cd_{IN} and Cd_{OUT} configurations, it would be removed automatically in the analysis process. This is because the analysis relies on the difference between Cd_{IN} and Cd_{OUT}.

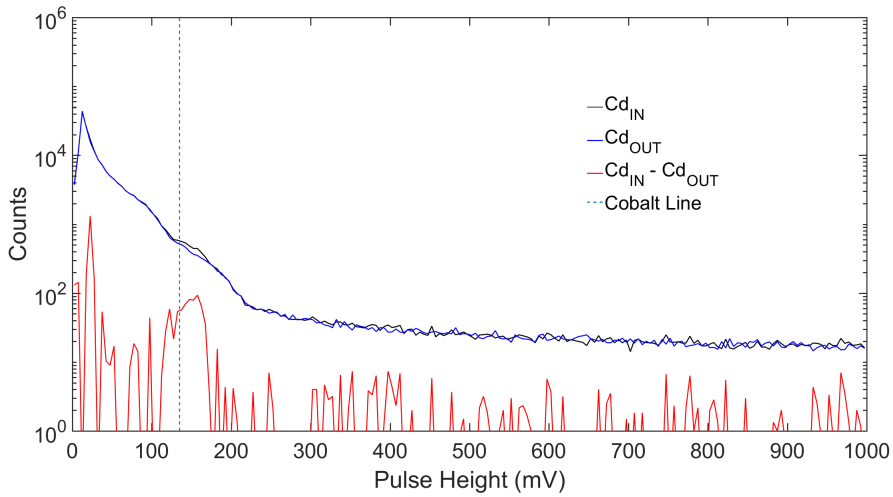

Figure 2.6 Thirty-minute background runs scaled to the normal run time (5 minutes) for Cd_{IN} and Cd_{OUT}. This shows that the pulse heights of most of the background events lie below the cobalt line. The red line is the difference between the two runs, and is nonzero most likely due to cosmic ray neutrons. This 'fake' neutron signal, though small, was used to correct our neutron detection rates.

Therefore, I checked the background contribution to the difference by taking thirty-minute background runs for Cd_{IN} and Cd_{OUT}. These runs and their difference are found in Figure 2.6. The difference is large enough to make background non-negligible. So, in the analysis of our data found in the results, we subtracted out the Cd_{IN} and Cd_{OUT} background rates from the respective runs, instead of assuming the subtraction of the two non-background runs would take care of background.

2.5.2 Monte Carlo Supplement

My advisor and I took an interest in discovering the rate at which we were acquiring signals from shielding gammas (see Eq. (1.1)). Since this is experimentally difficult to obtain, we implemented Monte-Carlo methods. The Monte Carlo N-Particle (MCNP) program was used to verify the data we collected and also obtain this shielding gamma rate. Using this rate, we could artificially separate the shielding gamma count from the fission gamma count, which counts are experimentally obtained in total, but not individually. Since shielding gammas come from neutron capture, they also contribute to our neutron signal, like with the neutron capture in cadmium. However, because this count is obtained through MCNP, it is not used in determining the intrinsic efficiency of the detector.

Chapter 3

Results & Discussion

The goal of the experiment was to measure how well our detector identifies fission. This measure was made in counts per fission for gamma rates and counts per neutron for neutron rates. Keeping the neutron count 'per neutron' makes the results independent of what source might have been used or might be present. Since energy is generally linear with pulse-height, we visualized our data with the pulse height spectra. This also allowed for adjusting the energy threshold from 10 mV (low threshold) to the DHS threshold (cobalt line or 135 mV). We determined our gamma ray counts from Cd_{OUT} runs and our neutron counts through Cd_{IN} runs minus Cd_{OUT} runs. The Cd_{OUT} counts are actually a combination of gamma ray counts (fission gammas, neutron capture gammas in the shielding, and neutron capture in the detector) and proton recoil counts, but the proton recoil count is assumed to be relatively small since the light output from such a reaction in PVT is an order of magnitude smaller. So, all of these events are lumped into our Cd_{OUT} counts. Monte Carlo methods (MCNP) were implemented to separate shielding gammas from the Cd_{OUT} counts. All these data were obtained through single-pulse analysis. Our ability to detect boron in the source shielding was realized through double-pulse analysis.

3.1 Single-Pulse Analysis

The focus of the single-pulse analysis was to determine how many fission-identifying counts we can see with our detector. The more gammas per fission and neutrons per neutron, the better our detector is at identifying fission. Thus, the gamma ray count and the neutron count are of import to us, not just the neutron count.

A couple of attributes make up a single-pulse event. First, the voltage must exceed the threshold and stay above it for at least 4 channels, which corresponds to 16 nanoseconds. For every such pulse, the pulse height is recorded. These features are found in Figure 3.1. The threshold for our events was 7.5 mV, which corresponds to 0.11 MeV (assuming linear relationship between pulse-height and particle energy). The data could be re-analyzed for counts above different thresholds.

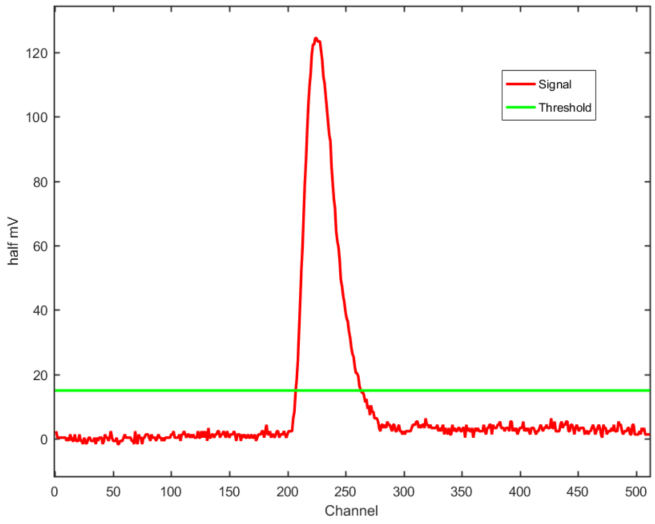

Figure 3.1 Waveform for a single-pulse event. Our digitizer waits for the voltage to reach threshold and stay above threshold for 4 channels (16 nanoseconds). When these criteria are met, the digitizer saves out 512 channels of data, with the trigger nearly centered in the event window. For every singles event, we focused on the pulse height.

A visual interpretation of the data is my first objective. The runs with cadmium on the face of the detector are the black lines in Figure 3.2. The blue lines are counts for runs without the

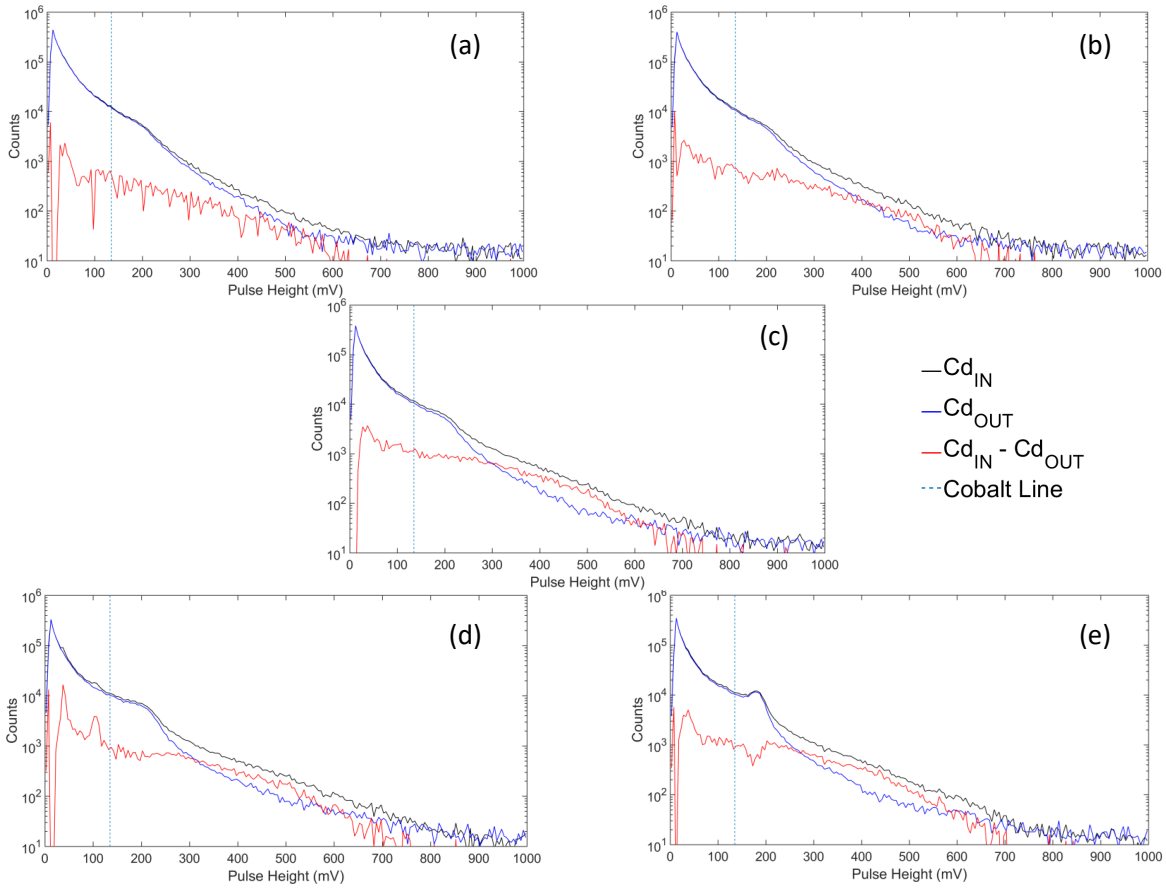

Figure 3.2 Pulse height histograms for (a) bare ^{252}Cf source and paraffin wax shielding of diameters (b) 6.48 cm, (c) 12.41 cm, (d) 20.4 cm, and (e) 23.5 cm. The run with the cadmium sheet is in black, the run with cadmium sheet removed in blue, and the difference between these two runs in red. The cobalt line is the vertical line. The difference between the Cd_{IN} and Cd_{OUT} shows the neutron signal.

cadmium. The difference between these two runs is primarily due to the neutrons from the fission source. Therefore, the neutron signal is given by the difference, which is the red line in the plots. The blue dashed line is the cobalt line.

The interesting trend to note is that the region between the blue and black lines opens up with increasing shielding diameter. This suggests that the neutron count is generally increasing with shielding diameter. Another point of interest is that no matter the shielding diameter, the total counts (black) is quite large for both thresholds.

The quantitative results confirm the visual cues. Tables 3.1 and 3.2 display the numeric results for the various shielding diameters at the two thresholds (10 mV and 135 mV). The low threshold is the lowest practical threshold and includes the most data. Though it is not above the cobalt energies, the neutron count comes from the difference between Cd_{IN} and Cd_{OUT}, which is assumed to be already 'blind' to cobalt. Table 3.2 shows the count rates above the cobalt threshold, which demonstrates the detector's abilities in compliance with DHS requirements, though these requirements don't fit well with our method.

Table 3.1 Single-pulse analysis results with low threshold (10 mV) for the various shielding diameters.

Shielding Diameter (cm)	Cd_{IN} Counts[a]	Cd_{OUT} Counts[a]	Cd_{IN} - Cd_{OUT} Counts[b]
Bare	8.60	8.48	0.0324
6.48	8.42	8.17	0.0653
12.61	7.90	7.52	0.1004
20.4	7.48	6.97	0.1351
23.5	7.44	7.02	0.1112

[a] Detected in a 4π detector per fission event

[b] Detected in a 4π detector per fission neutron

These data are competitive. Table 3.3 illustrates how these data compare to a commercial product and the ANSI standard. Again, since cadmium captures neutrons to produce signals in our detector, the cadmium gammas column represent our detector's neutron detection capability. The first two columns sum to what our detector sees without cadmium. The separation of those two data are possible only through theoretical calculations (MCNP). But with this separation, we can see that neutron signals (shielding and Cd gammas) total to competitive values, especially at

Table 3.2 Single-pulse analysis results with high threshold (135 mV) for the various shielding diameters. These results are completely above cobalt energies, thus ensuring the fulfillment of the DHS cobalt requirements.

Shielding Diameter (cm)	Cd_{IN} Counts[a]	Cd_{OUT} Counts[a]	Cd_{IN} - Cd_{OUT} Counts[b]
Bare	0.739	0.676	0.0169
6.48	0.716	0.606	0.0294
12.61	0.850	0.643	0.0550
20.4	0.966	0.774	0.0510
23.5	0.960	0.754	0.0547

[a] Detected in a 4π detector per fission event

[b] Detected in a 4π detector per fission neutron

shielding diameters that are realistic. For example, the total neutron signals per fission in a 4π detector at 20.4 cm shielding diameter is 0.973 and 1.01 for 23.5 cm. These results confirm that neutron counts per fission generally increase for increased shielding diameter. Though our detector does not represent a revolutionary neutron detector, including the gamma ray signals makes it a great fission detector. The sum of the BYU columns represents counts per fission that identify fission (not neutrons or gammas individually). These sums are an order of magnitude larger than that of Symetrica and the ANSI standard.

Table 3.3 Comparison of gamma and neutron detection capabilities between our experimental setup and other well known standards and work. The shielding gammas and the Cd gammas can be seen as our neutron detection capability, which at higher shielding compares well with the others. With increasing shielding, our signal goes up, while the others will drop significantly from loss of neutrons in the shield. The ability to see the fission gammas is unique to our detector, which adds great capability to detect fission events, not just neutrons.

Shielding Diameter (cm)	BYU Fission gammas [a]	BYU Shielding gammas [a]	BYU Cd gammas [a]	Symetrica neutrons [a]	ANSI Standard neutrons [a]
Bare	8.48	0	0.121	···	···
6.48	8.17	0.008	0.245	0.864	0.847
12.61	7.36	0.162	0.377	···	···
20.4	6.50	0.466	0.507	···	···
23.5	6.43	0.594	0.418	···	···

[a] Detected in a 4π detector per fission event

3.2 Double-Pulse Analysis

Results surrounding boron detection in shielding were determined using double-pulse analysis. A couple of attributes make up a double-pulse event. First, events are saved out in exactly the same manner as in the single-pulse events; the only difference is that the time window is opened up to 20 μs. This allows enough time to possibly see a neutron capture gamma, which can follow up to roughly 20 μs after the fission occurs. Thus, ideally the first pulse would be a fission gamma hitting our detector, and the second pulse would be the neutron capture gamma. Since we were looking for neutron capture gammas from boron, we set an upper threshold on this second pulse at

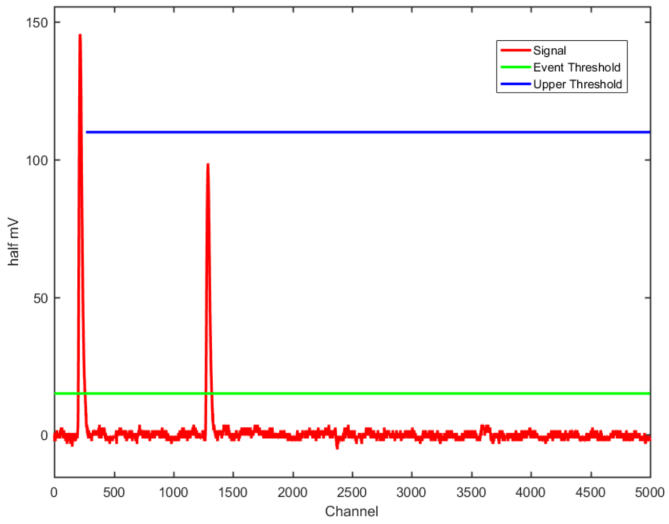

Figure 3.3 Waveform for a double-pulse event. Data taken with a 20 μs (5000 channels) event window were used to find doubles. Except for accidentals, the first pulse is the fission gamma and the second pulse is the neutron capture gamma. Thus, the time between the two pulses gives us an idea of how long it took for the neutron to capture.

a value just above the boron gamma ray (see Equation (1.2)). A doubles event with the described thresholds and features is shown in Figure 3.3. The threshold for our events was 7.5 mV, which corresponds to 0.11 MeV (assuming linear relationship between pulse-height and particle energy).

Since boron has a relatively large cross section for neutrons, boron captures neutrons quicker than hydrogen. This high cross section makes boron (especially the ^{10}B isotope) a great shielding element. But, since it captures quicker, a unique pile-up of capture gammas should occur at low time intervals. Thus, in double-pulse analysis, I focused on the time between the doubles in the event. This time interval is the time it took for the neutron to thermalize and capture. Our timing analysis was rather crude, as it was based on the time of the peaks of the pulses. More sophisticated timing techniques were deemed unnecessary for our purposes.

Histograms of the time-between-doubles for the various shielding thicknesses and types are found in Figure 3.4. These plots demonstrate the pile up at low time intervals when the shielding is

borated. The pure polyethylene line evidently lacks the unique shape of the borated polyethylene. Thus, this decay-like shape is unique to boron and potentially to other high cross-section elements. We therefore can "see" if boron is being used in the shielding.

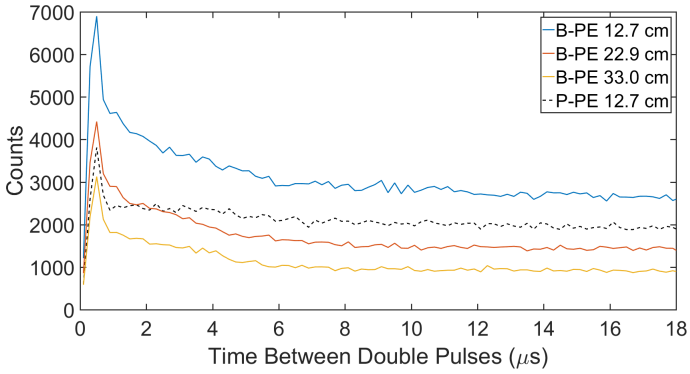

Figure 3.4 Time between pulse peaks in the case of doubles events. The three plots of the borated polyethylene (B-PE) show increased counts in the fast capture region (low time between). This confirms that boron's high cross-section for neutron capture effects a signature in this analysis. The pure polyethylene (P-PE) line shows that hydrogen captures fail to add up significantly in fast capture region, like boron. This analysis can be used to detect boron in the shielding, a sure sign of an attempt to hide neutrons.

This ability is still a simple visual test. A numerical test of the data to help solidify the concept still needs to be derived. This could be as simple as subtracting or taking the ratio of the two halves of the data. With this method, boron could be identified if the difference is quite positive, especially in the time zone of 1 μs to 8 μs (critical time zone). This difference is represented by the filled areas in Figure 3.5 and is shown with the ratios in Table 3.4. Note that the difference for all borated runs have relatively large counts in the critical time zone. It is fortunate that this trend holds for the various thicknesses of shielding. This is important since shielding thickness is unknown when scanning at ports.

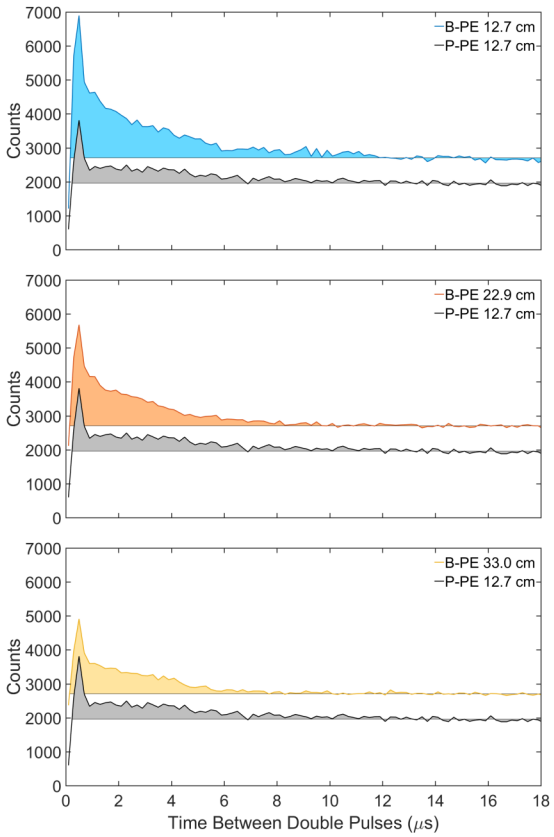

Figure 3.5 A graphical analysis of borated polyethylene (B-PE) versus pure polyethylene (P-PE). Each boron run has been vertically offset and paired with the one pure polyethylene run. One approach to identify boron in neutron shielding could be to subtract the last 9 μs from the first and look for the decay-rate-like signature of boron. The filled areas represent this difference. The boron runs stick out in comparison with pure polyethylene. Numerical analyses can help differentiate between 12.7 cm P-PE and 33.0 cm B-PE. This technique is one way to identify boron in the shielding.

This aspect of the research can be improved. First, more data would be useful. It would be interesting to see how pure polyethylene looks for shielding thicknesses that match the other two borated shielding thicknesses. Also, the timing methods used in the analysis are very rudimentary. Constant fraction timing could be used to improve the precision in the results. Finally, a more robust numerical technique for identifying boron in the data can be developed. The concept nevertheless holds. This detector can see boron, a blinding obstacle for gamma-insensitive detectors.

Table 3.4 Example of numerical analysis of borated vs non-borated shielding.

Shielding Type & Diameter (cm)	Difference (counts microseconds)	Ratio
B-PE 12.7	5433.8	1.279
B-PE 22.9	3767.4	1.360
B-PE 33.0	2605.2	1.390
P-PE 12.7	2134.0	1.151

Difference and ratio are between first half (1 μs - 8 μs) and second half (11 μs - 18 μs)

3.3 Summary

Our PVT detector has unique detection capabilities. Pulse height spectra of californium for various shielding diameters reveal plenty of events, even above the cobalt threshold. The neutron signal, obtained from Cd_{IN} minus Cd_{OUT}, is decent in magnitude. The general upward trend in neutron signal with increasing shielding is very unique. The neutron signal flattens around 20.4 cm shielding diameter with a value of 0.13 neutrons per fission neutron. The overall fission signal total makes our signal around 7 fission signals per fission event in a 4π detector, an order of magnitude larger than many neutron detectors. Through double-pulse analysis, boron can be detected. Numerical techniques need to be developed to solidify the detection of boron in the shielding.

In practice, the detector could be used according to the the following description. As you only have a short time window to scan cargo before you interrupt the flow of commerce, there is a series of flags that lead to the alarm. First, begin scanning with the cadmium sheet on. have the pulse height spectrum grow in real time (during the scan). If counts do not significantly pile up above background for any threshold after two minutes, then the cargo may continue. If, however, there are a lot of events, then this is the first flag. This signifies that someone is shipping something with

high gamma-emission rates and possibly neutrons. To continue the investigation after the first flag, take another two minutes of data with the cadmium sheet removed. If the counts are significantly lower than the first run, then flag two has been found. This would signify neutrons. If needed, re-analyze data to look for the boron signature in the doubles timing as discussed earlier. If it is present, then this is the third and final flag. This means that (1) there are neutrons and (2) boron is being used to hide them. The combination of flag one and two is enough to be alarmed, but flag three leaves no doubt that there is a fission source and that there is an intent to minimize emissions.

Appendix A

Configuration of CAEN Digitizer

Below is the text file used to configure the CAEN DT5720 digitizer in preparation to acquire data. The text below is for the single-pulse analysis. The changes that were made to it for the double-pulse analysis data are listed in Section 2.5.

```
% BYU Pulse Waveform Recorder Configuration File
% ----------------------------------------------------------------
% Settings common to all channels
% ----------------------------------------------------------------
[COMMON]

% OPEN: open the digitizer
% options: USB 0 0      Desktop/NIM digitizer through USB
%          USB 0 BA     VME digitizer through USB-V1718 (BA = BaseAddress of the VME board, 32 bit hex)
%          PCI 0 0 0    Desktop/NIM/VME through CONET (optical link)
%          PCI 0 0 BA   VME digitizer through V2718 (BA = BaseAddress of the VME board, 32 bit hex)
%OPEN USB 0 0
%OPEN USB 0 32100000
OPEN PCI 0 0 0
%OPEN PCI 0 0 32100000

% DAC_SLOPE: scales the dc offset for the dac
% Range 0.5 to 2.0
% DAC_SLOPE 1.0 % DT5720 s\n 31
DAC_SLOPE 1.19 % DT5720 s\n 79


% DAC_INTERCEPT: dac offset for calibrating the dc offset
% Range -1000 to 1000
% DAC_INTERCEPT 0 % DT5720 s\n 31
DAC_INTERCEPT 610 % DT5720 s\n 79

% DIRECTORY: directory to write data files to (full path, no slash at the end). 100 characters max length
DIRECTORY D:\Bart\Bart&Ashton\PVT_Californium\

% EXTENSION: data file extension (include the dot). 10 characters max length
EXTENSION .dat
```

```
% TOTAL_SECONDS: number of seconds to stop digitizing after. Choose 0 for continuous run
TOTAL_SECONDS 300

% TOTAL_EVENTS: number of collected events to stop digitizing after. Choose 0 for continuous run
TOTAL_EVENTS 0

% EVENTS_PER_FILE: number of events to be written to file before creating a new file to write to
EVENTS_PER_FILE 3000000

% POST_TRIGGER: post trigger size in percent of the whole acquisition window
% options: 0 to 100
% On models 742 there is a delay of about 35nsec on signal Fast Trigger TR; the post trigger is added to this delay
POST_TRIGGER  50

% RECORD_LENGTH = number of samples in the acquisition window
RECORD_LENGTH  512

% EXTERNAL_TRIGGER: external trigger input settings. When enabled, the ext. trg. can be either
% propagated (ACQUISITION_AND_TRGOUT) or not (ACQUISITION_ONLY) through the TRGOUT
% options: DISABLED, ACQUISITION_ONLY, ACQUISITION_AND_TRGOUT
EXTERNAL_TRIGGER DISABLED

% ENABLE_ZLE: enable zero length encoding (set individual channel thresholds below)
% options: YES, NO
ENABLE_ZLE NO

% MAX_NUM_EVENTS_BLT: maximum number of events to read out in one Block Transfer. High values corresponds to
% options: 1 to 1023
MAX_NUM_EVENTS_BLT 1023

% USE_INTERRUPT: number of events that must be ready for the readout when the IRQ is asserted.
% Zero means that the interrupts are not used (readout runs continuously)
USE_INTERRUPT 1

% MEM_BUFFERS: number by which CAEN internal memory is to be divided.
% Options: 0 to 10, where 0x00 is 1, 0x01 is 2, 0x02 is 4, 0x03 is 8, ... 0x0A is 1024.
MEM_BUFFERS 0

% FPIO_LEVEL: type of the front panel I/O LEMO connectors
% options: NIM, TTL
FPIO_LEVEL  NIM

% TEST_PATTERN: if enabled, data from ADC are replaced by test pattern (triangular wave)
% options: YES, NO
TEST_PATTERN   NO

% ------------------------------------------------------------------
% Individual Settings
% ------------------------------------------------------------------

% The following settings are applied specific to each channel.
%
% ENABLE_INPUT: enable/disable one channel
% Options: YES, NO
%
% DC_OFFSET: DC offset is in increments of approximately 2/65536 volts %
% Options: -2047.00 to 2047.00.
%
% TRIGGER_EDGE: rising or falling edge for trigger
% Options: RISING or FALLING
%
% TRIGGER_THRESHOLD: threshold for the channel auto trigger (ADC counts)
% are expressed in increments of 2/4096 volt. To specify zero volts use
% 2047.  For 1.0 volt use 4095 and -1.0 volt use 0.
% Options: -2047 to 2047.
%
% CHANNEL_TRIGGER: sets the channel trigger to one of three modes when enabled:
% options: DISABLED, ACQUISITION_ONLY, ACQUISITION_AND_TRGOUT
%
% ZLE_THRESHOLD: zero length encoding voltage threshold. All samples not exceeding
% threshold voltage are discarded (except Pretrigger and Posttrigger samples).
% options -2047 to 2047.
```

```
%
% ZLE_LOGIC: POSITIVE keeps samples over ZLE_THRESHOLD and NEGATIVE keeps samples
% under ZLE_THRESHOLD.
% Options: POSITIVE or NEGATIVE.
%
% ZLE_PRE_THRESHOLD: number of samples to keep before ZLE_THRESHOLD is true.
% Options: 0 to 65535.
%
% ZLE_POST_THRESHOLD: number of samples to keep after ZLE_THRESHOLD goes false.
% Options: 0 to 65535.

[0]
ENABLE_INPUT YES
CHANNEL_TRIGGER ACQUISITION_ONLY
DC_OFFSET 162
TRIGGER_EDGE FALLING
TRIGGER_THRESHOLD -15
MIN_TRIG_WIDTH 4
ZLE_THRESHOLD -100
ZLE_POLARITY NEGATIVE
ZLE_PRE_THRESHOLD 10
ZLE_POST_THRESHOLD 10

[1]
ENABLE_INPUT NO
CHANNEL_TRIGGER DISABLED
DC_OFFSET 157
TRIGGER_EDGE FALLING
TRIGGER_THRESHOLD -250
MIN_TRIG_WIDTH 4
ZLE_THRESHOLD 2040
ZLE_POLARITY NEGATIVE
ZLE_PRE_THRESHOLD 10
ZLE_POST_THRESHOLD 10

[2]
ENABLE_INPUT NO
CHANNEL_TRIGGER DISABLED
DC_OFFSET 106
TRIGGER_EDGE FALLING
TRIGGER_THRESHOLD 250
MIN_TRIG_WIDTH 4
ZLE_THRESHOLD 2040
ZLE_POLARITY NEGATIVE
ZLE_PRE_THRESHOLD 10
ZLE_POST_THRESHOLD 10

[3]
ENABLE_INPUT NO
CHANNEL_TRIGGER DISABLED
DC_OFFSET 154
TRIGGER_EDGE FALLING
TRIGGER_THRESHOLD 0
MIN_TRIG_WIDTH 4
ZLE_THRESHOLD 2000
ZLE_POLARITY POSITIVE
ZLE_PRE_THRESHOLD 10
ZLE_POST_THRESHOLD 10

[4]
ENABLE_INPUT            NO
CHANNEL_TRIGGER         DISABLED
DC_OFFSET               139
TRIGGER_EDGE FALLING
TRIGGER_THRESHOLD       -10
MIN_TRIG_WIDTH 75
ZLE_THRESHOLD 2000
ZLE_POLARITY POSITIVE
ZLE_PRE_THRESHOLD 10
ZLE_POST_THRESHOLD 10

[5]
```

```
ENABLE_INPUT            NO
CHANNEL_TRIGGER         DISABLED
DC_OFFSET               0
TRIGGER_EDGE FALLING
TRIGGER_THRESHOLD       0
MIN_TRIG_WIDTH 4
ZLE_THRESHOLD 2000
ZLE_POLARITY POSITIVE
ZLE_PRE_THRESHOLD 10
ZLE_POST_THRESHOLD 10

[6]
ENABLE_INPUT            NO
CHANNEL_TRIGGER         DISABLED
DC_OFFSET               33
TRIGGER_EDGE FALLING
TRIGGER_THRESHOLD       0
MIN_TRIG_WIDTH 4
ZLE_THRESHOLD 2000
ZLE_POLARITY POSITIVE
ZLE_PRE_THRESHOLD 10
ZLE_POST_THRESHOLD 10

[7]
ENABLE_INPUT            NO
CHANNEL_TRIGGER         DISABLED
DC_OFFSET               45
TRIGGER_EDGE FALLING
TRIGGER_THRESHOLD       0
MIN_TRIG_WIDTH 4
ZLE_THRESHOLD 2000
ZLE_POLARITY POSITIVE
ZLE_PRE_THRESHOLD 10
ZLE_POST_THRESHOLD 10
```

Bibliography

[1] R. T. Kouzes, E. R. Siciliano, J. H. Ely, P. E. Keller, and R. J. McConn, "Passive neutron detection for interdiction of nuclear material at borders," Nuclear Instruments and Methods in Physics Research Section A: Accelerators, Spectrometers, Detectors and Associated Equipment **584,** 383–400 (2008).

[2] G. F. Knoll, *Radiation detection and measurement*, 4th ed. ed. (John Wiley, Hoboken, N.J., 2010).

[3] C. Higgins, "Cadmium Capture-gated Neutron Detector Analysis of the U-235 Fission Spectrum," (2014).

[4] A. Corey, "Construction and Testing of Four Adit Photomultiplier Tubes With Scintillating Plastic for Neutron Detection," (2014).

[5] B. Ostler, "Minimizing Room Return Neutrons," (2016).

Index